Multichannel contributions in the nonsequential double ionization of CO$_2$

M. Oppermann,[1] S. J. Weber,[2,1] L. J. Frasinski,[1] M. Yu. Ivanov,[3,1] and J. P. Marangos[1]

[1]*Department of Physics, Imperial College London, South Kensington Campus, London SW7 2AZ, United Kingdom*
[2]*CEA-Saclay, IRAMIS, Service des Photons, Atomes et Molecules, 91191 Gif-sur-Yvette, France*
[3]*Max Born Institute, Max Born Strasse 2a, 12489 Berlin, Germany*

The intermediate molecular states in the double ionization of molecules by laser-driven electron recollision are encoded into the angular-dependent signature of the process. We identify through this signature the specific ionic states participating in the double-ionization mechanism. Using CO$_2$ as an example we employ a 1350-nm strong field at 2×10^{14} W cm^{-2} to ensure that nonsequential double ionization (NSDI) is the exclusive mechanism in CO$_2^{2+}$ formation. Under these conditions we obtain two main results. First, the shape of the recolliding electron wave packet is inferred from measurements of the ellipticity dependence of the signal, and second, the inelastic recollision cross section in the molecular frame is extracted from the variation of the signal as a function of the angle between strong-field probe polarization and molecular axis. These results provide an angularly resolved electron-ion collision measurement in CO$_2$ and demonstrate contributions to NSDI from both ground and first excited ionic states.

I. INTRODUCTION

Laser-driven electron recollision [1] has been identified as a unique tool for imaging molecular structure and ultrafast internal dynamics. Via high harmonic generation, it has been employed in the molecular frame to identify specific ionization channels and track subsequent hole dynamics [2,3]. High harmonic generation is exclusively driven by recollision; in contrast, molecular double ionization (DI) and fragmentation caused by inelastic recollisions compete with direct laser-field-induced processes. This typically complicates the control of inelastic recollision phenomena and so inhibits the extraction of information on molecular structure and dynamics.

Here we use a long-wavelength drive field to ensure that nonsequential double ionization (NSDI) is the only route to CO$_2^{2+}$. We fully characterize the inelastic rescattering event by measuring the shape of the returning electron wave packet and the recollision cross section in the molecular frame. This allows us to unambiguously identify the contribution of different ionic states due to their distinct orbital symmetry. Our results also provide an angularly resolved electron-ion collision measurement in CO$_2$, which is not possible through traditional crossed beam scattering experiments.

DI may proceed either (a) sequentially (sequential double ionization; SDI), via two independent laser-induced ionization events, or (b) nonsequentially, where the secondary ionization is caused by inelastic recollision (NSDI) [4]. In the latter case the two ionization events and ejected electron wave packets are correlated and thus enable study of the multielectron dynamics in the parent ion [5]. NSDI has been identified in CO$_2$ with 800-nm fields [6] and differential ion recoil momentum (COLTRIMS) studies have revealed the angular dependence of recollision-induced dissociative DI [7]. The latter approach is used mostly to study repulsive final states from which the molecular alignment can be reconstructed, since the study of meta-stable doubly charged ions requires additional active molecular alignment in the laboratory frame. This has thus far only been realized in the case of N$_2$, but only parallel and perpendicular rates with respect to the molecular axis were compared [8].

NSDI requires tunneling ionization (TI) as the initial step, which sensitively depends on the molecular structure. Here, the angular TI rate scales approximately with the electronic density profile of the respective molecular orbital along the ionizing laser polarization direction [9]. Due to the exponential dependence of the TI rate on the ionization potential I_p it might be assumed that the ionization channel via the highest occupied molecular orbital (HOMO) is dominant. It is well known, however, that lower lying orbitals may contribute significantly to the ionization mechanism in appropriately aligned molecules, even at moderate intensities, due to strong geometrical factors in the ionization rate [10,11].

The maximum recollision energy the freed electron can acquire in a laser field with intensity I and wavelength λ is $E \approx 3.17 U_p$, where $U_p \propto I\lambda^2$ is its ponderomotive energy [1]. NSDI requires recollision energies high enough to overcome the second ionization potential I_p^+. In practice, NSDI will only be the dominant DI mechanism at intensities well below the single-ionization (SI) saturation threshold; otherwise, sequential channels will dominate. We show that by increasing the driving laser wavelength from 800 to 1350 nm, both of the above criteria are met. In this case the second ionization event is a laser-driven electron-ion collision which is sensitive to the molecular structure of the ionic valence orbital.

In the molecular frame the channels contributing to NSDI can be identified via their associated orbital symmetry. This can be achieved in two ways. First, a nodal plane aligned along the linear laser polarization direction leads to destructive interference between the components of the recolliding wave packets with opposite transverse momentum components in the polarization plane [12]. This manifests itself in a maximum NSDI yield for nonzero laser ellipticity [13]. Second, the node in the electronic density profile of the parent ion leads to a local minimum in the angularly resolved recollision cross section. By measuring the ejected electron wave packet and the corresponding recollision cross section, we use independent measurements of both ellipticity and alignment dependence in

a linearly polarised field to characterize the NSDI dynamics in CO_2.

This paper is organized as follows. Section II details our experimental setup and the experimental results are presented in two complementary parts: Sec. III A highlights the behavior of NSDI as a function of ellipticity, while Sec. III B presents its angular behavior and extraction of the recollision cross section. These results are then discussed in Sec. IV, where evidence of multichannel contribution to NSDI is shown. Finally, we conclude with Sec. V.

II. EXPERIMENTAL SETUP

The experiment was conducted in a single-stage time-of-flight (TOF) mass spectrometer operated under Wiley-McLaren focusing conditions [14]. This approach was more compact than COLTRIMS and allowed us to work with denser gas samples and so provided the much higher data acquisition rate required for this study. Additional laser-induced molecular alignment allowed us to measure the angularly dependent yield of fragments with zero kinetic energy release (e.g., CO_2^{2+}), which are not accessible to COLTRIMS. Differential pumping ensured background pressures in the interaction region below 8×10^{-8} mbar during gas jet operation with 2.3 bar backing pressure. The sample was delivered in the form of a molecular beam and consisted of 40% CO_2 mixed in Ar. The use of mixed gases had several advantages for the experiment: (a) it increased rotational cooling of the sample and thus improved the degree of molecular alignment [15], and (b) the Ar^+ signal was used for monitoring laser intensity fluctuations which could be accounted for in the data analysis.

The collinear pump-probe setup is illustrated in Fig. 1. A linearly polarized, 800-nm, 75-fs alignment pulse at 5×10^{13} W cm^{-2} prepared a rotational wave packet. A typical half-revival, recorded under these conditions, is displayed in
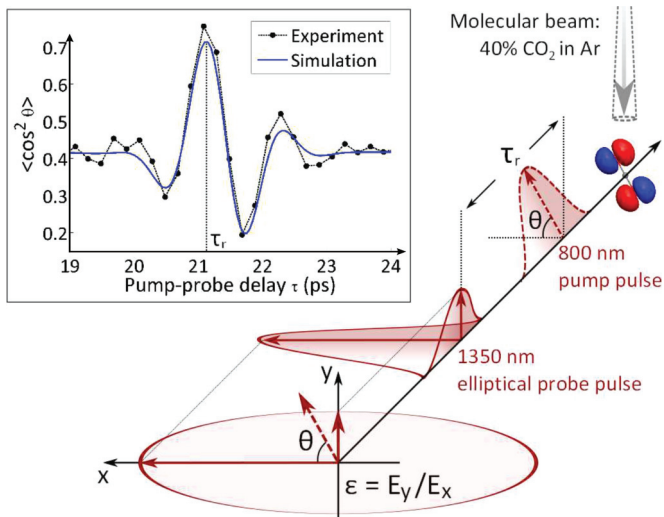

FIG. 1. (Color online) Pump-probe scheme for investigating the ellipticity and polarization dependence of NSDI in impulsively aligned CO_2. Ions were detected via a TOF spectrometer operated in Wiley-McLaren mode. Inset: Half-revival of the rotational wave packet induced by the pump pulse under the employed experimental conditions.

the inset in Fig. 1. At the indicated pump-probe delay τ_r, an alignment quality of $\langle \cos^2 \theta \rangle = 0.71$ was extracted from simulations (for details see [15]). Here, the molecular sample was aligned along the alignment pulse polarization and probed with 1350- or 800-nm, 30-fs pulses at 2×10^{14} W cm^{-2}. They were obtained from a commercial optical parametric amplifier (He-TOPAS; Light Conversion) pumped by a commercial Ti:sapphire CPA system (Red Dragon; KM Labs) or directly from the CPA system. An achromatic half-wave plate rotated the alignment pulse polarization and thus the molecular axis with respect to the probe pulse. For ellipticity measurements, an achromatic quarter-wave plate manipulated the polarization state of the probe pulse. Rotations of the associated polarization ellipse were compensated by the rotation of the alignment pulse polarization.

The laser pulses were focused via a 25-cm-focal-length lens, leading to focal spot diameters of 52 ± 4 and 53 ± 4 μm for the probe and alignment pulse, respectively. The laser intensities were estimated via the measured pulse parameters and confirmed via saturation intensity measurements in Ar [16]. Pulse durations were measured as intensity full width at half-maximum (FWHM) via a commercial NIR SPIDER (APE) and a home-built IR SPIDER. Ion yields were recorded via a multichannel plate detector and a fast digital storage oscilloscope (DPO7254; Tektronix).

III. RESULTS

A. Ellipticity behavior

We first established recollision as the exclusive DI mechanism. In Fig. 2 the ellipticity dependence of CO_2^{2+} at 2×10^{14} W cm^{-2} for 800 and 1350-nm fields is compared. Ion yields were recorded as a function of ellipticity ϵ for three values of θ, denoting the angle between the molecular axis and the major axis of the probe polarization ellipse. For 800 nm, only the ellipticity curve for $\theta = 45°$ is shown. The half width at half-maximum (HWHM) $\Delta\epsilon$ for each curve
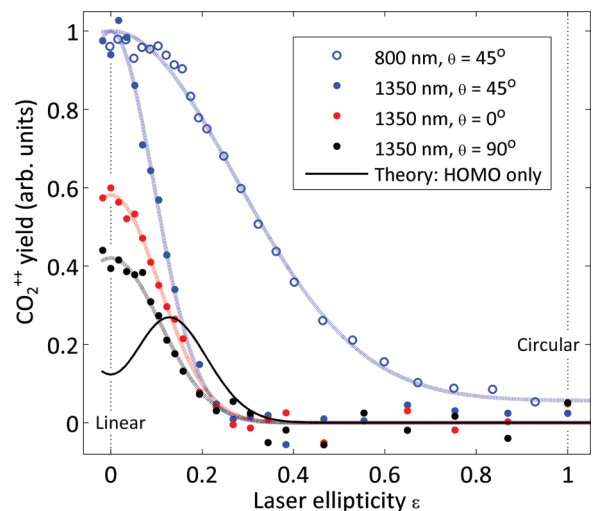

FIG. 2. (Color online) CO_2^{2+} yield as a function of driving laser ellipticity ϵ comparing 800 and 1350 nm at an intensity of 2×10^{14} W cm^{-2}. θ denotes the angle between the molecular bond axis and the major axis of the laser polarization ellipse.

is obtained via the Gaussian fits displayed in the figure and result in $\Delta\epsilon_{800} = 0.29 \pm 0.02$ and $\Delta\epsilon_{1350} = 0.12 \pm 0.02$. The most important observation is the significantly reduced $\Delta\epsilon$ for 1350 nm, such that the signal vanishes for all alignment angles at $\epsilon > 0.3$. The same behavior was observed for high harmonic generation in atoms [17] and CO_2 [12] (which we know is produced via electron recombination following recollision) and for DI of Ar in this experiment (data not displayed). We thus conclude that at 1350 nm, CO_2^{2+} is exclusively produced via NSDI, while at 800 nm a significant SDI contribution is still present. This motivated us to concentrate all subsequent measurements on the 1350-nm case.

Under these conditions, the ellipticity curves map out the transverse velocity distribution of the recolliding electron wave packet ([13] and references therein). However, if NSDI takes place along a nodal plane in the molecular orbital, recollision is expected to be suppressed for linear polarization due to quantum interferences. This should become visible as a dip in the ellipticity dependence at $\epsilon = 0$, with the major axis of ellipticity along the node similar to the results of Bhardwaj *et al.* [13] on benzene molecules. For the HOMO of CO_2, this effect is thus expected to be most strongly pronounced at $\theta = 90°$.

We developed therefore a phenomenological model (see Appendix) to infer this behavior. We calculated the double-ionization-yield ellipticity dependence and convolved it with the experimentally obtained alignment distribution of the molecular sample. The resulting curve [solid black line in Fig. 2, taken from Fig. 7(c), 90° case] thus estimates the ellipticity dependence of NSDI from HOMO under the employed experimental conditions. It displays a strong suppression at $\epsilon = 0$, with a maximum NSDI yield at $\epsilon_{max} \approx 0.13$. The associated experimental data (filled black circles in Fig. 2), however, does not display this behavior. It reaches its maximum at $\epsilon_{max} = 0$ and is described well by a Gaussian dependence. This is the case at all employed values for θ and the extracted $\Delta\epsilon$ are found to agree within the quoted error. The measured ellipticity dependence and its model seems to hint at a multichannel contribution of NSDI in CO_2, i.e., not via the HOMO channel alone. Moreover, these measurements confirm that the transverse momentum distribution of the electron wave packet has predominantly the form of a structureless Gaussian for all molecular alignments. This suggests the contribution of a lower orbital, which does not have a nodal plane for $\theta = 90$. This assumption is further supported by the independent results presented in the next section.

B. Recollision cross section

Contributions to NSDI from lower lying orbitals may be identified via its angular dependence. The associated polarization-dependent ionization rates are displayed in Fig. 3. There, CO_2^{2+} and total CO_2^+ yields and their ratio are shown as a function of θ (the angle between the strong-field and the alignment-field polarizations) with $\epsilon = 0$. The total CO_2^+ yield is obtained by adding all ion yields that result from the parent ion, including fragment ions from dissociative SI. Each data curve is normalized with respect to the maximum value of the associated polynomial fit.
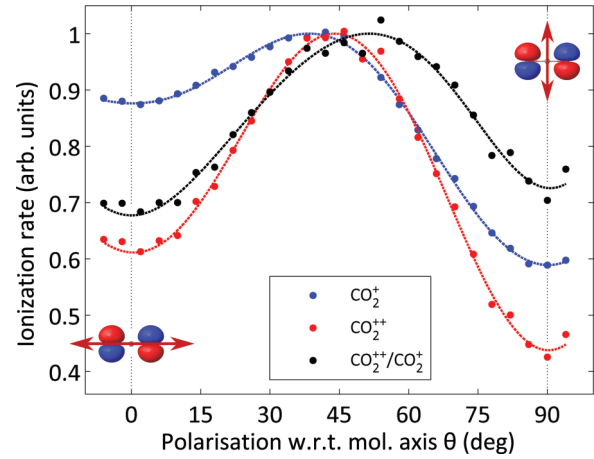

FIG. 3. (Color online) Total CO_2^+ and CO_2^{2+} yields and their ratio as a function of the angle θ between the linear laser polarization and the molecular axis for 1350 nm and 2×10^{14} W cm^{-2}. Lines were obtained from polynomial fits.

The measured SI rate is suppressed for parallel and perpendicular polarization, while this effect is significantly stronger for perpendicular alignment. The rate reaches a maximum at $\theta_{max}^{SI} = 39° \pm 1°$, with the error estimated from the variation of the fit with polynomial order. This agrees well with recent calculations for the angular-dependent direct ionization rate from HOMO of CO_2, where a maximum was found at $\theta_{max}^{SI} = 40°$, with the strongest ionization suppression for perpendicular polarization [11]. Due to its π_u symmetry (see Fig. 4), contributions from the next lower lying orbital HOMO-1 would lead to an increase in ionization rate for perpendicular polarization. There, ionization suppression would be reduced and the location of the maximum shifted to $\theta_{max}^{SI} > 40°$. We thus conclude that in this experiment, SI is strongly dominated by the HOMO.

The angularly resolved NSDI rate displays significant differences from the SI rate. The maximum is found at $\theta_{max}^{NSDI} = 44° \pm 1°$ and suppression for parallel polarization is distinctly stronger compared to SI. This suggests that
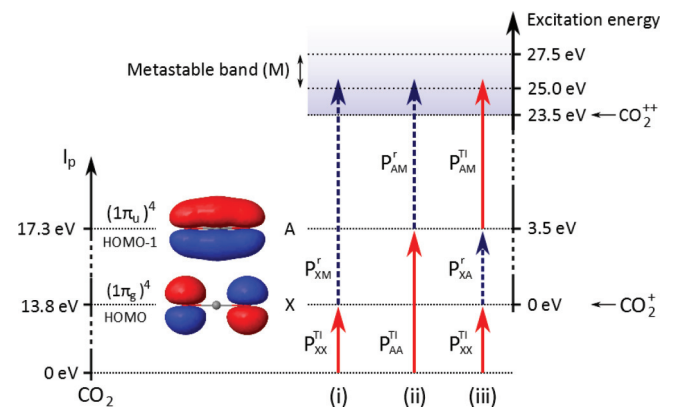

FIG. 4. (Color online) Schematic of the three channels considered for NSDI in this experiment. Solid arrows denote tunneling ionization; dashed arrows, inelastic recollision. Note that the ionization continuum of the parent ion is reached at 23.5 eV with respect to the ionic ground state [20].

the angular-dependent recollision cross section $\sigma^r(\theta)$ differs significantly from the SI cross section $\sigma^{\text{SI}}(\theta)$. Assuming that the propagation of the free electron in the continuum has a negligible effect on the angular dependence of NSDI (as supported by our ellipticity measurements), its cross section can be approximated to fulfill $\sigma^{\text{NSDI}}(\theta) \propto \sigma^{\text{SI}}(\theta) \times \sigma^r(\theta)$. In this case, the full angularly resolved recollision cross section $\sigma^r(\theta)$ can be experimentally deduced from the ion yield ratio CO_2^{2+}/CO_2^{+} and is displayed in black in Fig. 3.

IV. DISCUSSION

During an inelastic recollision the free electron interacts with the bound electrons in the parent ion. One may thus assume that for sufficiently high recollision energies the angular cross section of this process approximately scales like the electron density profile of the parent ion. As in the case of TI, the shape of $\sigma^r(\theta)$ therefore contains information about the ionic states involved in the NSDI mechanism. In a Koopman-type picture, the orbital symmetry of the parent ion corresponds to the orbital of the neutral from which the electron has been removed. This means that TI from HOMO leads to the molecular ion in the ground state X with the same orbital symmetry. TI from HOMO-1 is then associated with the first excited state A.

Comparing $\sigma^r(\theta)$ to $\sigma^{\text{TI}}(\theta)$ now allows for further characterization of the recollision step in terms of the contributing ionic states. Most notably in $\sigma^r(\theta)$, suppression for parallel polarization is stronger than for SI, while the opposite is true for perpendicular alignment. Furthermore, the maximum cross section is reached at $\theta_{\max}^r = 52° \pm 1°$. The observed differences between $\sigma^r(\theta)$ and $\sigma^{\text{SI}}(\theta)$ show that the recollision step does not possess the same angular symmetry as TI from HOMO. In the Koopman picture this implies that NSDI of CO_2 cannot be understood by restricting its mechanism to the ionic ground state X. This agrees with the ellipticity measurements and we therefore conclude that the measured $\sigma^r(\theta)$ identifies clearly the contribution of excited ionic states to NSDI in CO_2.

Analogously to the discussion of $\sigma^{\text{SI}}(\theta)$, $\theta_{\max}^r > 40°$ implies the contribution of the first excited ionic state A. Three NSDI channels to CO_2^{2+} involving HOMO (X state) and HOMO-1 (A state) and their corresponding ionic states X and A can be considered: (i) TI from X followed by impact ionization of the ionic X state, (ii) TI from X followed by impact ionization of the ionic A state, and (iii) TI from X followed by recollision excitation with subsequent field ionization [18] via the ionic A state. They are illustrated in Fig. 4. Channel (i) would display an angular dependence like SI from X. Due to the π_u symmetry of the first excited ionic state, contributions from channels (ii) and (iii) would then lead to an increased cross section for perpendicular polarization, shifting the location of the maximum towards larger angles. In the case of CO_2, the next higher lying excited ionic states B and C are not suitable for explaining the observed recollision cross section due to their orbital symmetry and dissociative behavior [19].

The reason for the pronounced contribution of the ionic state A cannot, however, be simply due to an increased probability of channels (ii) and (iii) with respect to (i). This is due to their lower TI rates P_{AA}^{TI} and P_{AM}^{TI} and the fact that the long-driving laser wavelength leads to a high maximum recollision energy,

such that $E_{1350} \approx 109$ eV (compared to $E_{800} \approx 38$ eV). This implies that all three channels are open. We therefore suggest that channels (ii) and (iii) are strongly pronounced in the NSDI mechanism due to preferential formation of CO_2^{2+} ions in a band of metastable states. This band has been found to consist of the first three excited states of CO_2^{2+} [20]. Ionization from the first excited state of CO_2^{+} is thus more likely to produce meta-stable CO_2^{2+} ions than ionization from the ground state.

V. CONCLUSION

In summary, we have identified multichannel contributions to molecular NSDI. For this, we angularly resolve the inelastic recollision event in CO_2 by measuring the shape of the recolliding electron wave packet and the angular recollision cross section in the molecular frame. We then identify the ionic ground and first excited state as the main NSDI channels via their associated orbital symmetries. Our results also demonstrate the feasibility of measuring the angular dependence of electron-molecular ion collisions, albeit over a finite energy range, which is not readily accessible with existing methods. The universal applicability of this method thus demonstrates the potential of using inelastic recollisions in the molecular frame of reference for extracting and controlling molecular dynamics.

APPENDIX: NSDI ELLIPTICITY BEHAVIOR

This Appendix presents a phenomenological model for describing the influence of orbital nodal planes on the yield of NSDI (for more detailed discussion of this topic see [21]). It takes into account that CO_2 has two degenerate HOMO orbitals, Π_x and Π_y, each with two nodal planes. The first step in our model is tunnel ionization from these orbitals. If one considers a perfectly aligned CO_2 molecule in the plane defined by the molecular axis and the probe laser polarization, then only one orbital will lead to nonzero ionization and recollision [22]. This is depicted in Fig. 5. Note that this plane is a nodal plane for the other orbital. Consequently the ionization and recollision event can be restricted to this two-dimensional plane.

The remaining orbital has two nodal planes at $0°$ and $90°$ with respect to the molecular axis. This leads to a net zero recollision probability along these planes due to destructive interference of the electron wave packet. However, Bhardwaj and coworkers [13] showed that an elliptically polarized laser field can be used to counteract this interference effect. This leads to an enhanced NSDI yield at nonzero laser ellipticity.
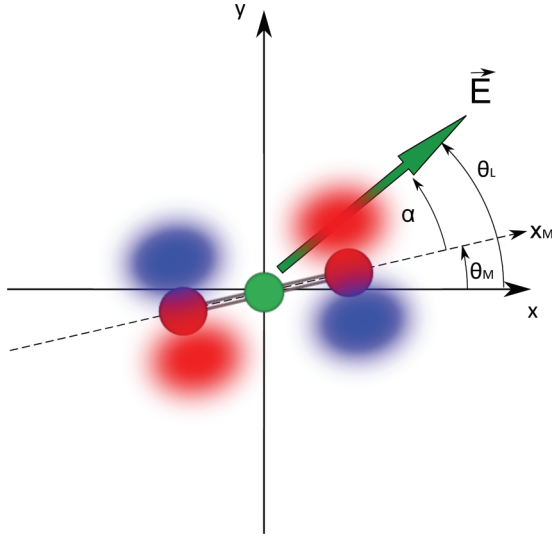
FIG. 5. (Color online) CO_2 HOMO aligned at an angle θ_M with respect to the x axis (set as the alignment axis) and probed by an electric field $\vec{E}$ at an angle θ_L with respect to alignment axis and α with respect to the molecular axis.

The purpose of our model is to estimate the ellipticity dependence of NSDI when only the HOMO orbital and its two nodal planes are taken into account.

There are two limiting cases for the ellipticity dependence of NSDI in an aligned molecule, with the laser polarization (i) along a maximum of the electronic probability density (P^+) and (ii) along a nodal plane of the orbital (P^-),

$$P^+(\epsilon) = \frac{1}{N^+} e^{-(\epsilon/\epsilon_0^+)^2},$$
$$P^-(\epsilon) = \frac{\epsilon^2}{N^-} e^{-(\epsilon/\epsilon_0^-)^2},$$

(A1)

with $N^\pm$ normalization constants. P^+ is obtained from the momentum transverse distribution of the electron wave packet after tuneling through a barrier [23]. Furthermore, a classical trajectory calculation leads to a transverse momentum of $v_\perp \approx \epsilon \frac{F}{\omega_L}$ for an electron recolliding to the core in an elliptical field. P^+ is maximum for zero ellipticity, while P^- is maximum for $\epsilon > 0$. ϵ_0^+ was extracted from the experimental CO_2^{2+} ellipticity measurement. $\epsilon_0^- = 0.7\epsilon_0^+$ was set to match the total yield of $P^+(\epsilon)$ at an ellipticity of 0.3, where recollision was measured to be switched off.

Their relative angular probability $w^\pm$ depends on the probing angle α of the laser field relative to the molecular axis. Qualitatively, one expects the sole contribution of P^- along the nodal planes where destructive interference of the wave packet takes place. Its contribution should then vanish quickly with increasing α. Here we use parametric functions to describe this behavior:

$$w^-(\alpha) = |\cos\alpha|^n + |\sin\alpha|^n,$$
$$w^+(\alpha) = 1 - w^-(\alpha),$$

(A2)

where the exponent n can be set to represent a sharp probability around $0°$ and $90°$ with $n \approx 50$ or a smoother one with $n \approx 10$. The w^- (w^+) distribution is represented as a black dashed
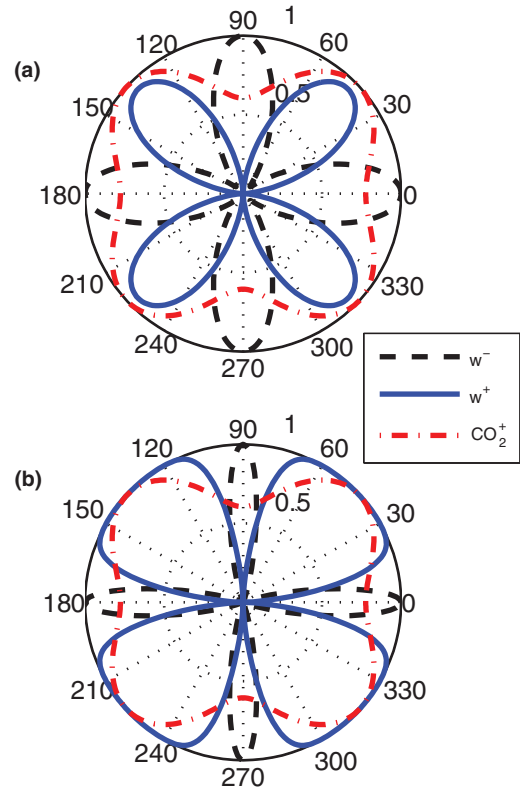

FIG. 6. (Color online) Polar plot (in degree) of w^- (resp. w^+) distribution (defined by Eq. (A2)) (black dashed curve, resp. blue solid curve) for $n = 10$ in (a) and $n = 50$ in (b). The red dash-dot curve is the deconvolved single ionization yield $\Theta(\alpha)$.

(blue solid) line for $n = 10$ in [Fig. 6(a)] and for $n = 50$ in [Fig. 5(b)].

The total angular and ellipticity dependence of the recollision event is then given by

$$P_{\text{tot}}(\alpha,\epsilon) = \Theta(\alpha)[w^-(\alpha)P^-(\epsilon) + w^+(\alpha)P^+(\epsilon)], \quad (A3)$$
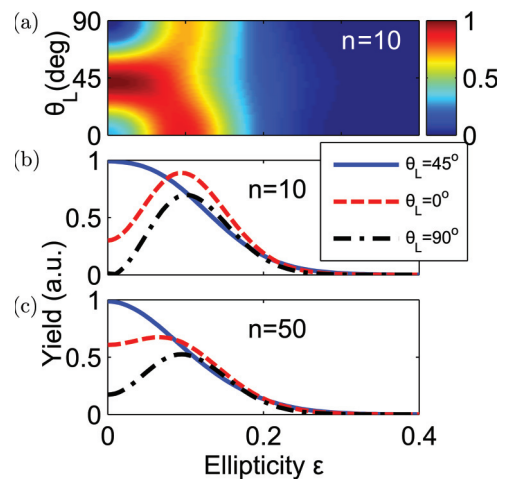

FIG. 7. (Color online) (a) Convolved $P_{\text{tot}}(\alpha,\epsilon)$ distribution with the molecular angular distribution at the half revival for n = 10. (b) Lineouts of (a) for $\theta_L = 0°$, $45°$ and $90°$. (c) Lineouts of the same distribution for $n = 50$.

where we have multiplied the angular distributions by the deconvolved CO_2^+ SI rate Θ, obtained from the experiment (see dot-dashed (red) curve in Fig. 6; for the deconvolution see [21]).

This distribution was calculated for a molecule fixed in space at a single angle. During an experiment, however, this is impossible to achieve and we must account for an angular distribution. Laser-induced nonadiabatic molecular alignment creates a rotational wave packet that can be probed at its half-revival with the highest probability of having the molecules aligned along a fixed axis (here the x axis). However, there is a nonzero probability of molecules being aligned slightly off this axis. To take this into account, we retrieved all the parameters of the impulsive alignment and rotational temperature during the experiment [15] and processed an alignment simulation to obtain the probability density of molecular alignment, $\rho(\theta_M)$. The final angular distribution was obtained by convolving P_{tot} with this molecular angular distribution [21].

Figure 7 shows the final angular and ellipticity dependence of our NSDI model for $n = 10$ [Figs. 7(a) and 7(b)] and for $n = 50$ [Fig. 7(c)]. Figures 7(b) and 7(c) are line-outs of the two-dimensional distribution for the major axis of the probe laser's polarization ellipse at $\theta_L = 0°$, $45°$, and $90°$ to be compared with the experimental ellipticity yield. In both cases a strong suppression of NSDI for zero ellipticity is visible, while the curves peak at $\epsilon \approx 0.1$. This effect is strongest for $\theta_L = 90°$ and should therefore be visible in the experiments if only the HOMO orbital is contributing to the total NSDI yield.

The results confirm that the measured ellipticity dependence of NSDI cannot be explained by taking only the HOMO orbital into account. This suggests that orbitals with another symmetry such as HOMO-1 must be included to correctly account for the observed data on ellipticity dependence.

[1] P. B. Corkum, Phys. Rev. Lett. **71**, 1994 (1993).

[2] O. Smirnova *et al.*, Nature **460**, 972 (2009).

[3] R. Torres *et al.*, Phys. Rev. A **81**, 051802 (2010).

[4] D. N. Fittinghoff *et al.*, Phys. Rev. Lett. **69**, 2642 (1992).

[5] H. Niikura *et al.*, Nature **421**, 826 (2003).

[6] L. Pei *et al.*, Phys. Rev. A **82**, 021401 (2010).

[7] A. S. Alnaser *et al.*, Phys. Rev. A **71**, 031403 (2005).

[8] D. Zeidler *et al.*, Phys. Rev. Lett. **95**, 203003 (2005).

[9] X. M. Tong *et al.*, Phys. Rev. A **66**, 033402 (2002).

[10] D. Pavicic *et al.*, Phys. Rev. Lett. **98**, 243001 (2007).

[11] L. Torlina *et al.*, Phys. Rev. A **86**, 043409 (2012).

[12] T. Kanai *et al.*, Phys. Rev. Lett. **98**, 053002 (2007).

[13] V. R. Bhardwaj *et al.*, Phys. Rev. Lett. **87**, 253003 (2001).

[14] W. C. Wiley *et al.*, Rev. Sci. Instr. **26**, 1150 (1955).

[15] M. Oppermann *et al.*, Phys. Chem. Chem. Phys. **14**, 9785 (2012).

[16] S. M. Hankin *et al.*, Phys. Rev. A **64**, 013405 (2001).

[17] K. S. Budil *et al.*, Phys. Rev. A **48**, R3437 (1993).

[18] B. Feuerstein *et al.*, Phys. Rev. Lett. **87**, 043003 (2001).

[19] R. Bombach *et al.*, J. Chem. Phys. **79**, 4214 (1983).

[20] A. Slattery *et al.*, J. Chem. Phys. **122**, 084317 (2005).

[21] S. J. Weber, M. Oppermann, M. Yu. Ivanov, and J. P. Marangos, J. Mod. Opt. (2013), doi: 10.1080/09500340.2013.814925.

[22] M. Abu-samha and L. B. Madsen, Phys. Rev. A **80**, 023401 (2009).

[23] M. Y. Ivanov, M. Spanner, and O. Smirnova, J. Mod. Opt. **52**, 165 (2005).